

1 Supporting Information

2 for

3 **Ammonium chloride associated aerosol liquid water enhances haze in**

4 **Delhi, India**

5 **Ying Chen<sup>1,2,3\*</sup>, Yu Wang<sup>4</sup>, Athanasios Nenes<sup>5,6</sup>, Oliver Wild<sup>1</sup>, Shaojie Song<sup>7,8</sup>,**  
6 **Dawei Hu<sup>9</sup>, Dantong Liu<sup>10</sup>, Jianjun He<sup>11</sup>, Lea Hildebrandt Ruiz<sup>12</sup>, Joshua S. Apte<sup>13</sup>,**  
7 **Sachin S. Gunthe<sup>14,15\*</sup>, Pengfei Liu<sup>16\*</sup>**

8 <sup>1</sup>Lancaster Environment Centre, Lancaster University, Lancaster, LA1 4YQ, UK

9 <sup>2</sup>College of Engineering, Mathematics and Physical Sciences, University of Exeter, EX4 4QE, UK

10 <sup>3</sup>Laboratory of Atmospheric Chemistry, Paul Scherrer Institut (PSI), Villigen, 5232, Switzerland

11 <sup>4</sup>Institute for Atmospheric and Climate Science, ETH Zurich, Zurich, 8006, Switzerland

12 <sup>5</sup>School of Architecture, Civil & Environmental Engineering, École Polytechnique Fédérale de  
13 Lausanne, Lausanne, 1015, Switzerland

14 <sup>6</sup>Center for the Studies of Air Quality and Climate Change, Institute of Chemical Engineering  
15 Sciences, Foundation for Research and Technology Hellas, Patras, 26504, Greece

16 <sup>7</sup>John A. Paulson School of Engineering and Applied Sciences, Harvard University, Cambridge,  
17 MA, 02134, USA

18 <sup>8</sup>College of Environmental Science and Engineering, Nankai University, Tianjin, 300071, China

19 <sup>9</sup>Centre for Atmospheric Sciences, Department of Earth, Atmospheric and Environmental Sciences,  
20 University of Manchester, Manchester, M13 9PS, UK

21 <sup>10</sup>Department of Atmospheric Sciences, School of Earth Sciences, Zhejiang University, Hangzhou,  
22 Zhejiang, 310058, China

23 <sup>11</sup>State Key Laboratory of Severe Weather & Key Laboratory of Atmospheric Chemistry of CMA,  
24 Chinese Academy of Meteorological Sciences, Beijing, 100081, China

25 <sup>12</sup>McKetta Department of Chemical Engineering, The University of Texas at Austin, Austin, TX,  
26 78712, USA

27 <sup>13</sup>Department of Civil and Environmental Engineering, UC Berkeley, CA, 94720, USA

28 <sup>14</sup>EWRE Division, Dept. of Civil Engineering, Indian Institute of Technology Madras, Chennai,  
29 600036, India

30 <sup>15</sup>Laboratory for Atmospheric and Climate Sciences, Indian Institute of Technology Madras,  
31 Chennai, 600036, India

32 <sup>16</sup>School of Earth and Atmospheric Sciences, Georgia Institute of Technology, Atlanta, GA, 30318,  
33 USA

34 \*Correspondence to: Ying Chen (y.chen6@exeter.ac.uk), Pengfei Liu (pengfei.liu@eas.gatech.edu)  
35 and Sachin S. Gunthe (s.gunthe@iitm.ac.in)

36

37 **Contents of this file**

38

39 **Texts:**

40 Section S1– Aerosol water inhibits PBL development

41

42 **Tables:**

43 Table S1 – Concentration of secondary inorganic aerosol in each season.

44 Table S2 – Parameters of fitted functions in Fig. 3a;

45

46 **Figures:**

47 Figure S1 – Cross correlation matrix between ALWC and different factors;

48 Figure S2 – Ion balance in Delhi;

49 Figure S3 – Overview of data availability in Delhi;

50 Figure S4 – Mass fraction of each component in different pollution levels;

51 Figure S5 – SOR and NOR as a function of ALWC;

52 Figure S6 – Relationship between ALWC and inorganic and organic aerosols;

53 Figure S7 – Relationships between  $PM_{10}$ , ALWC and meteorology.

54

55

56

## 57 Section S1: Aerosol water inhibits PBL development

58 We perform analysis in the morning (7-11 a.m.) in winter and spring to demonstrate  
59 that aerosol water can significantly inhibit the development of the PBL in Delhi. These  
60 periods are chosen because: 1) concentrations of ALWC and pollutants are high in these  
61 seasons with a strong peak in the morning as shown in Fig. 2a; 2) PBL development is  
62 mainly driven by solar heating in the morning but could be influenced by additional  
63 factors such as surface latent heat in the afternoon<sup>1</sup>; and 3) observations of aerosol  
64 optical depth (column-integrated light extinction) are available from Terra-MODIS at  
65 around 10:30 a.m. local time. In order to quantify the ALWC-induced reduction in  
66 downward surface solar radiation and the corresponding inhibition of PBL development,  
67 we perform two steps. First, we use the NCAR-TUV radiation model to calculate the  
68 surface solar radiation given the aerosol optical depth from Terra-MODIS, which  
69 observes column light extinction due to ambient aerosol including the associated water.  
70 We further calculate the surface solar radiation in the absence of aerosol water,  
71 assuming that PBL is well mixed and the column  $f(RH)$  is the same as that at the surface.  
72 This is a reasonable assumption given that most of the particulate matter is constrained  
73 within the PBL which is only 200-300 m deep in winter and spring at the Terra-MODIS  
74 observation time (see Fig. 2c). The ALWC-induced reduction in surface solar radiation  
75 can be estimated from the difference between the calculations. The total column ozone  
76 loading, aerosol single scattering albedo and surface albedo are considered in the TUV  
77 calculations, as detailed in the Methods section. Secondly, we derive a function to  
78 describe the relationship between downward surface solar radiation and PBL height in  
79 winter and spring, using ERA5 reanalysis. A good relationship ( $R^2 > 0.7$ ) is found as  
80 shown in Fig. S7d and S7e. This relationship is used with the ALWC-induced solar  
81 radiation reduction derived above, to quantify the suppression of PBL height. It is worth  
82 noting that the ERA5 reanalysis does not consider non-sea-salt chloride and its  
83 associated water, and therefore the influence of ALWC on surface solar radiation and  
84 PBL height are not fully reflected in the ERA5 dataset. Nevertheless, it still represents  
85 the evolution of the PBL under surface heating from solar radiation, which is influenced  
86 by the climatological and surface physical characters<sup>1</sup>. The influence of ALWC on  
87 surface solar radiation is assessed in the first step and the PBL suppression is derived  
88 in the second step.

89  
90  
91  
92

93

**Table S1. Concentration of secondary water-soluble inorganic aerosol in each season.** The seasonal average mass concentration of each species in the liquid aerosol phase are estimated using the ISORROPIA model. Note that these species are present as ions in the liquid phase.

Units: $\mu\text{g}/\text{m}^3$	Spring	Summer	Monsoon	Winter
Ammonium sulphate	13.9	12.7	12.2	17.8
Ammonium nitrate	12.6	3.0	4.1	23.9
Ammonium chloride	18.4	1.9	0.6	27.0

94

95

**Table S2. Parameters of fitted functions**, in the form “ $y = \exp(a * x + b)$ ”, between RH and ALWC with respect to  $\text{PM}_{10}$  dry mass concentrations. The fitted curves are shown in Fig. 3a.

Data Groups	a	b	Data Number	R <sup>2</sup>
Cl fraction > 30%	0.099	-7.660	69	0.93
20% < Cl fraction $\leq$ 30%	0.080	-6.150	171	0.92
15% < Cl fraction $\leq$ 20%	0.077	-6.007	202	0.92
10% < Cl fraction $\leq$ 15%	0.079	-6.351	323	0.90
5% < Cl fraction $\leq$ 10%	0.076	-6.284	872	0.91
Cl fraction $\leq$ 5%	0.071	-6.000	2586	0.91

96

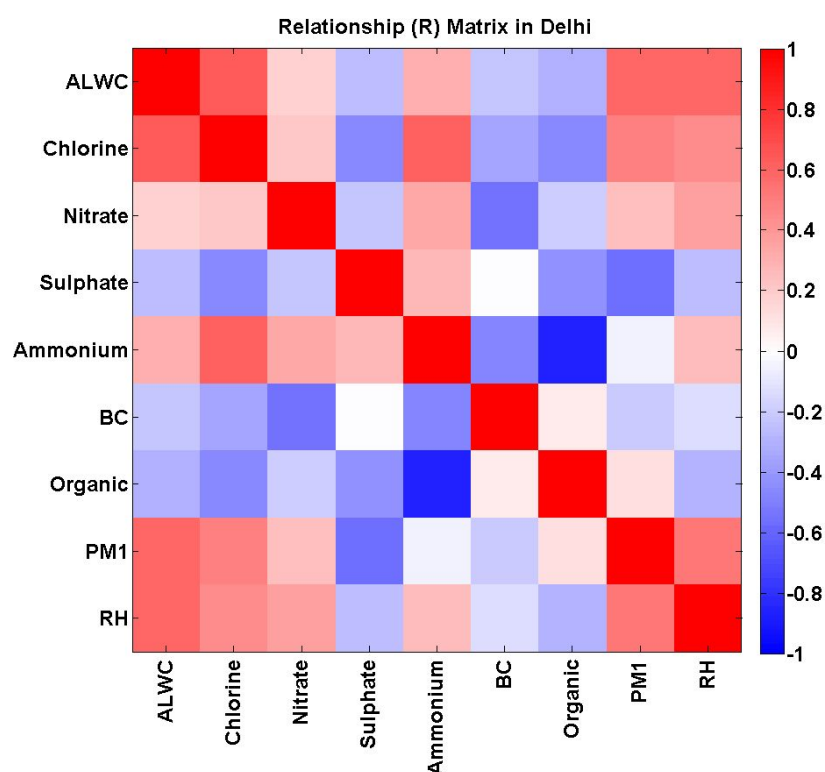


**Figure S1. Cross correlation matrix.** The colour indicates the correlation coefficient (R) between each pair. ALWC and  $\text{PM}_{10}$  represent the mass concentrations of aerosol liquid water content and particulate matter with diameter less than  $1 \mu\text{m}$ , and RH is the relative humidity. The mass fractions in  $\text{PM}_{10}$  of chlorine, nitrate, sulphate, ammonium, black carbon (BC) and organic are also shown.

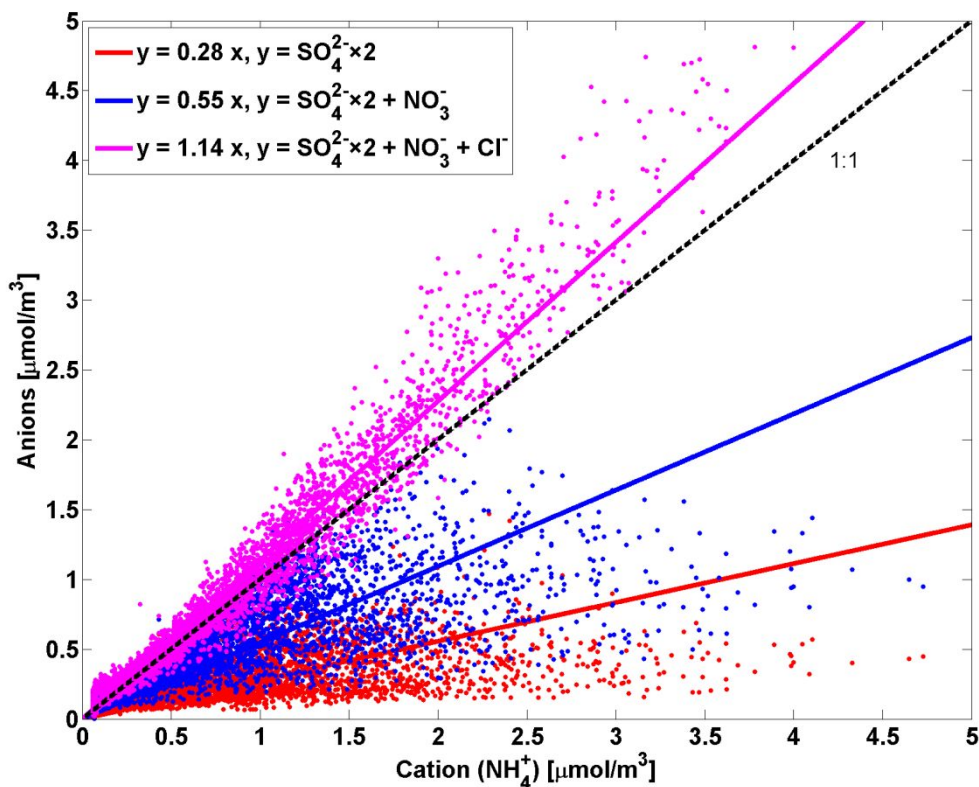


**Figure S2. Ion balance in Delhi measured by the ACSM.** The colored lines indicate anion-to-cation charge ratios for sulphate (red), sulphate + nitrate (blue), and sulphate + nitrate + chloride (purple), and the black dashed line denotes a 1:1 ratio.

97

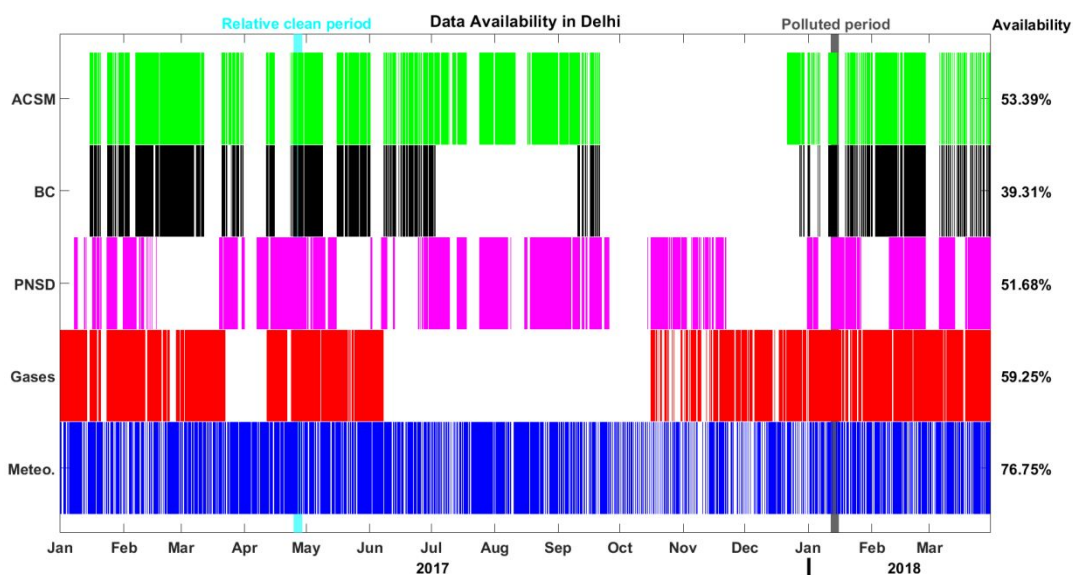


**Figure S3. Data availability of hourly observations in Delhi.** Non-refractory chemical composition observed by ACSM as shown in green, black carbon (BC) observed by AE33 in black, particle number size distribution (PNSD) in magenta,  $\text{SO}_2$  and  $\text{NO}_2$  concentrations in red, and meteorology in blue. The overall availability during the whole period, 2017-01-01 to 2018-03-31, is shown on the right side. The relatively clean period (light blue) and polluted period (grey) selected for analysis in Fig. 4 are also marked.

98  
99

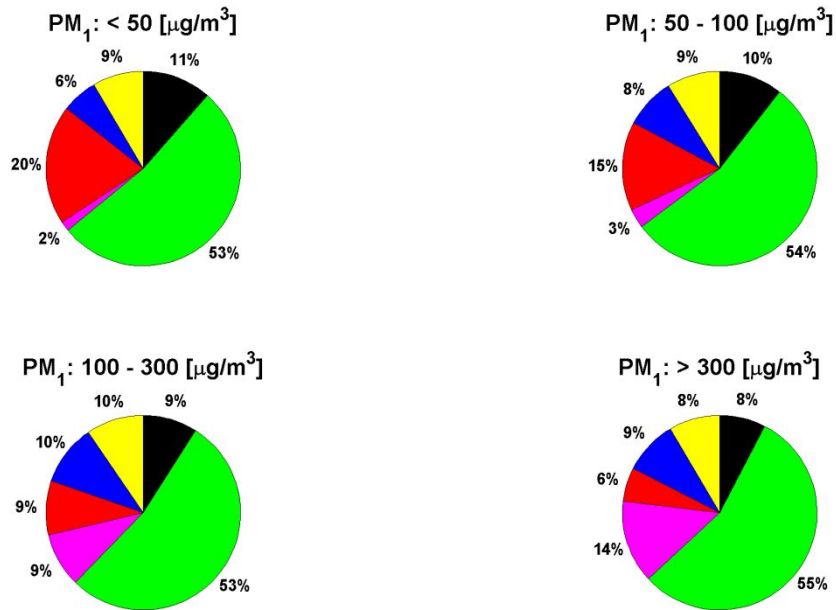


Figure S4. The mass fraction of each component in PM<sub>10</sub> at different pollution levels. Ammonium (yellow), nitrate (blue), sulphate (red), chlorine (magenta), organics (green) and black carbon (black).

100  
101

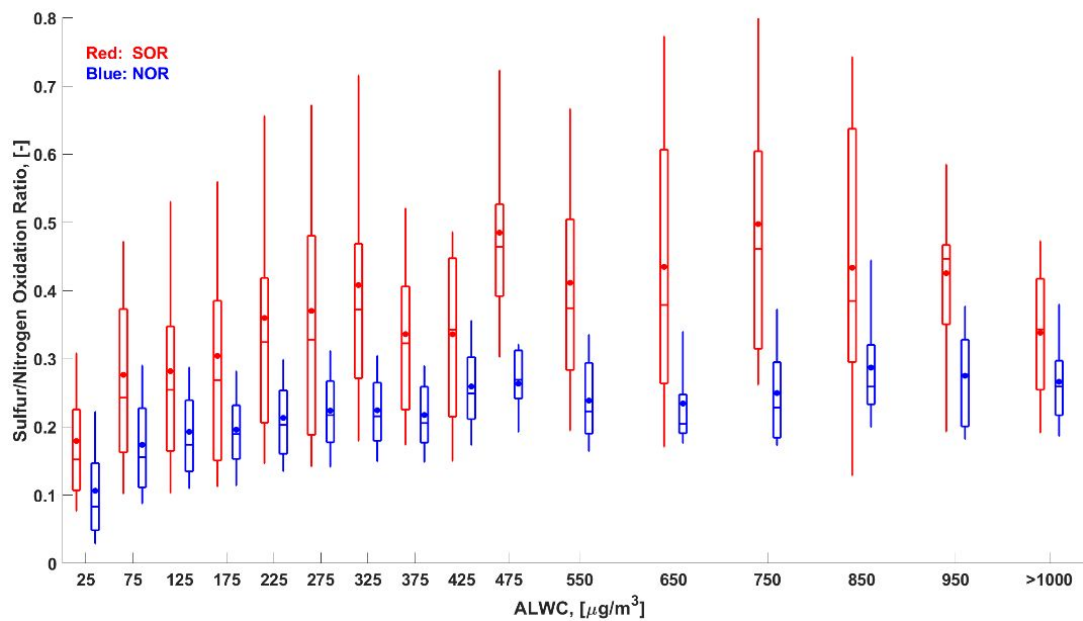


Figure S5. Relationship between aerosol liquid water content and sulfur or nitrogen oxidation ratio, i.e., SOR (red) or NOR (blue). The boxplots show 10<sup>th</sup>, 25<sup>th</sup>, median, 75<sup>th</sup> and 90<sup>th</sup> percentiles with the mean value indicated by a dot.

102  
103  
104

(b)

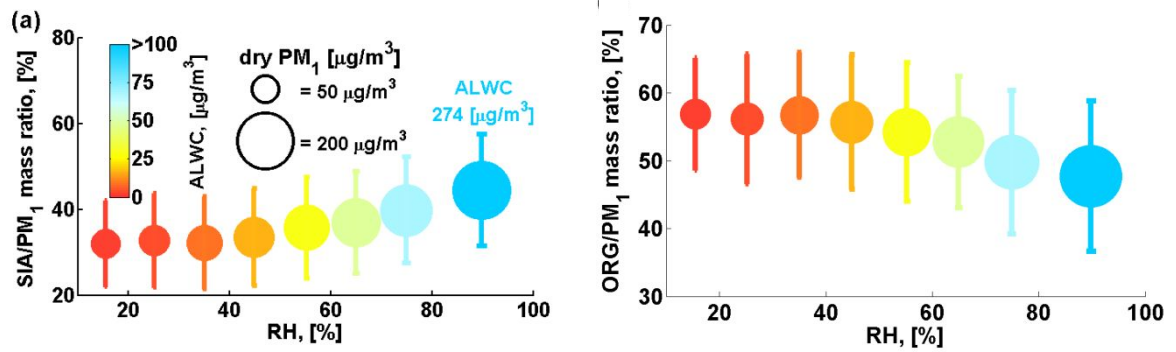


Figure S6. Similar to chloride in Fig. 3b, but showing the relationships between ALWC, RH and the mass fractions of total secondary inorganic (a) and organic (b) aerosols.

105

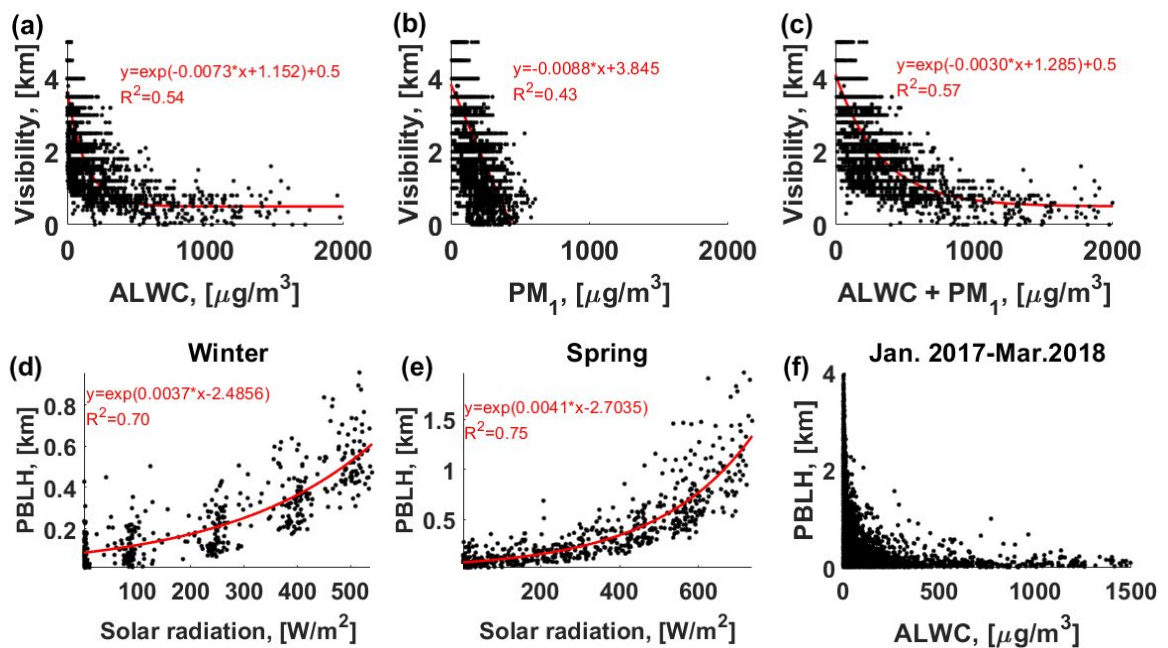


Figure S7. Relationship between  $PM_{10}$ , ALWC and meteorology. Visibility as a function of the mass concentration of ALWC (a),  $PM_{10}$  dry mass (b) and the sum of ALWC and dry  $PM_{10}$  (c). Planetary boundary layer height (PBLH) as a function of downward surface solar radiation during 7-11 a.m. in winter (d) and in spring (e), and as a function of ALWC (f).

106

107

108

**References:**

109

1. Medeiros, B.; Hall, A.; Stevens, B., What Controls the Mean Depth of the PBL? Journal of Climate 2005, 18, (16), 3157-3172.

110

111

112

113

114